J Mater Sci (2007) 42:2807–2819
DOI 10.1007/s10853-006-1379-7

Compressive creep behavior in air of a slightly porous as-sintered polycrystalline α-alumina material

Guillaume Bernard-Granger · Christian Guizard · Richard Duclos

Received: 2 November 2005 / Accepted: 22 February 2006 / Published online: 13 January 2007

Abstract Compressive creep tests in air have been performed on a polycrystalline submicron as sintered and slightly porous α-alumina material. Two different deformation mechanisms, depending on the applied stress and creep temperature, have been identified when the grain size becomes higher than a critical value $\langle G^{*} \rangle$.

For low temperatures and/or low applied stresses, deformation occurs by grain boundary sliding accommodated by an in-series ''interface reaction/diffusion of Al^{3+} cations'' process, with the limiting step being the interface reaction. In this case increased densification of the samples is observed after creep, compared to the as-sintered ones.

In contrast, for high temperatures and/or high-applied stresses, deformation occurs by grain boundary sliding accommodated by the relocation and growth of preexisting cavities, the growth step being also controlled by the diffusion of Al^{3+} cations. In this case, a marked decrease of the relative density is measured on the crept samples compared to the as-sintered ones.

Using these results, it is possible to identify the optimal conditions for superplastic forming of previously as-sintered parts, leading to shaped objects with an increased final density.

G. Bernard-Granger (✉) · C. Guizard
Laboratoire de Synthèse et Fonctionnalisation des Céramiques, FRE 2770 CNRS/Saint-Gobain, Saint-Gobain C.R.E.E., 84306 Cavaillon Cedex, France
e-mail: guillaume.bernard-granger@saint-gobain.com

R. Duclos
Laboratoire de Structure et Propriétés de l'Etat Solide, UMR CNRS 8008, Université des Sciences et Technologies de Lille, 59655 Villeneuve d'Ascq Cedex, France

Introduction

Polycrystalline α-alumina is one of the most commonly used ceramic materials in the industrial world. It has several well known key benefits: submicron raw powders are inexpensive relative to other fine ceramic materials; water based slurries are easily processed; various green shaping methods can be used; it sinters very well in air; and the obtained final room temperature properties of fired parts are very interesting when most of the porosity has disappeared. For example Vickers hardness is higher than 20 GPa [1, 2]; fracture toughness is ranging from 2.5 to 4.5 MPa $\sqrt{m}$ [3]; three-point flexural strength is between 600 and 850 MPa [1, 2]; it has a high resistance to diverse corrosive environments [4–6]; it exhibits an excellent wear resistance due to a low friction coefficient when alumina is in contact with alumina [3, 7, 8].

Of course, polycrystalline α-alumina has also some drawbacks, the primary one directly linked to its high hardness. Fully dense submicron polycrystalline alumina is extremely difficult to machine. One option is to green machine. However, if a zero crack-like defect microstructure is required, this process can introduce surface defects that may remain after sintering, even if a complementary hot isostatic pressing step is added.

An-other option to shape complex parts, having dimensions close to the final requirements and without any internal residual crack-like defects, is to use a high-temperature uniaxial superplastic forming technique. To determine the superplastic domain of a material (stress, temperature, deformation rate), creep tests have to be carry out. In the past, the superplastic behavior of several ceramics has been investigated: slightly doped alumina [9–12], alumina-zirconia

composites [13, 14], alumina-zirconia reinforced with SiC whiskers composites [15], zirconia [16–20], magnesium alumina spinel [21, 22], yttrium oxide [23, 24], silicon carbide [25], silicon nitride [26, 27] and complex composites [28]. At this time, despite extensive studies to identify the ideal parameters to superplastically shape different kind of materials, no significant industrial implementations have resulted due to low yields. The starting grain size after sintering may have been too high to obtain a high forming rate without damaging the microstructure.

Since powder makers are now able to produce α-alumina raw powders with an average initial grain size between 0.1 and 0.3 μm [29–30], it is possible to obtain polycrystalline α-alumina sintered parts with a relative density higher than 95% and a submicron average grain size [1, 2]. So, superplastic forming, using pre-sintered compacts, should again be considered as a potential near net shape solution when machining has to be limited.

In this study, the high-temperature compressive creep behavior of a slightly porous sintered, submicron, ultra pure α-polycrystalline alumina material has been investigated. In addition, the ideal conditions for uniaxial compression superplastic forming of near net shape final parts have been identified.

Experimental procedure

High solids loading (70 wt%) water based α-alumina slurries were prepared with a raw powder having a mean particle size of 0.2 μm (TM-DAR, Taimei Chemicals Co. Ltd, Tokyo, Japan). After optimal homogenization and degassing, samples were slip cast in porous molds.

Debindering (480 °C/3 h) and sintering runs (1,250 °C/3 h) were performed in air using a standard electrical furnace. Compacts with a final relative density equals to 97.2% were obtained (theoretical volume mass of alumina is 3.976 g/cm^3, it has been calculated from the elemental lattice structure). The volume mass of the samples was measured using an imbibition method with deionized water (three measurements were made for each sample, shown values are an average of the three measured values, standard deviation for the relative density values is ±0.1%).

The as-sintered microstructure was more precisely analyzed from fracture surfaces (to eliminate the possible grain growth occurring during thermal etching). The general microstructure of the as-sintered samples was characterized from SEM pictures, using a line intercept method taking into account at least 300 grains (with a three-dimensional correcting factor determined specifically to be 1.2).

Parallelepipeds were precisely machined for the creep tests from the as-sintered compacts. The size retained was $3 \times 3 \times 7$ mm^3.

Compressive creep tests were performed in air using temperatures in the range of 1,175–1,225 °C and stresses between 40 and 200 MPa. After recording the samples height variation during the experiments, the true strain is automatically calculated.

From the creep curves obtained, the creep rate $\dot{\varepsilon}$ has been automatically calculated point by point.

To be sure that all our creep tests were done with a constant true stress, the load was in all cases continuously corrected.

After the tests were performed, the deformed samples densities were measured using the same imbibition method with deionized water (three measurements for one sample, indicated values are an average of the three measured values, standard deviation for the relative density values is ±0.1%). In parallel, the precise dimensions of the crept samples were recorded to verify adequacy with the live continuously registered creep deformation.

Finally, the different crept microstructures were observed by SEM performed on fracture surfaces. As was done for the as-sintered material, the average grain size in the crept samples was determined using the same line intercept procedure.

To analyze the creep behavior of a specific polycrystalline material, the traditional Norton's law derived expression is usually used:

$$\dot{\varepsilon}_s = \frac{\partial \varepsilon}{\partial t} = A \frac{\sigma^n}{G^p} e^{-\frac{Q_d}{RT}} \quad (1)$$

where $\dot{\varepsilon}_s$ is the steady state creep rate, A is a constant, σ is the applied stress, n is the stress exponent, G is the material average grain size, p is the grain size exponent, Q_d is the activation energy for the mechanism controlling creep, R is the universal gas constant, and T is the absolute temperature.

In ceramic polycrystalline materials, grain growth usually occurs during the creep experiments at high temperature. Consequently the creep rate decreases continuously and no real steady state occurs which is why it is usually referred to as a pseudo steady state.

To determine which mechanism control creep deformation at high temperature, it is critical to determine the n, p and Q_d values from Eq. 1. Well-known differential methods were used for that.

To determine the n values, stress jumps were performed at a constant temperature, on a single sample which allows instantaneous grains size to be constant in the material.

Similarly, to determine the Q_d values, temperature jumps were performed at a constant creep stress, on a single sample. As before, this allows the instantaneous grains size to remain constant in the material.

Grain size, G, is a particular variable on which experimenters have not any influence during the creep experiments. As a result, the creep rates must be compared at the beginning and at the end of the tests, conditions under which the grains sizes can be easily measured. From relation (1), p is finally obtained as follows:

$$p = -\left[\frac{\ln\left(\frac{\dot{\varepsilon}_{\text{at creep end}}}{\dot{\varepsilon}_{\text{at creep beginning}}}\right)}{\ln\left(\frac{G_{\text{after creep}}}{G_{\text{before creep}}}\right)}\right]_{\sigma,T} \quad (2)$$

To have a precise starting basis for our study, Table 1 summarizes the principal different possible mechanisms controlling creep of ceramic polycrystalline materials at high temperature, with the corresponding values for n and p [31–37].

Experimental results

As-sintered material

After mirror polishing, thermal etching and SEM examinations, the typical microstructure of the as-sintered material can be seen in Fig. 1. Some residual pores, mostly distributed at the triple points formed by grain boundaries arrangement, are clearly observable. They are homogeneously dispersed in the bulk material.

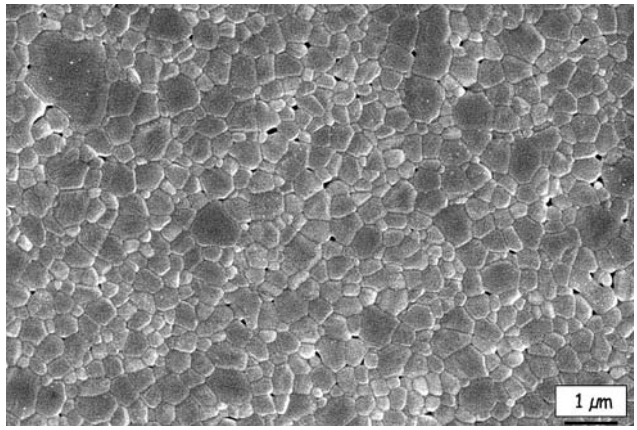

Fig. 1 Typical aspect of the as-sintered ultra pure alumina—D = 97.2%

From fracture and thermally etched mirror polished surfaces, the as-sintered microstructure was more precisely analyzed. It can be described as follows:

- Average corrected alumina grain size (or grain diameter) equal to 0.42 μm;
- Surface concentration of grains presenting abnormal growth equal to 3.5–4.0% (diameter of the concerned grains is at least two times the average corrected grain size).

At this time no evidence of an amorphous grain boundary phase has been observed.

In summary, the as-sintered polycrystalline α-alumina material is definitively composed of a submicron matrix, in which abnormal grains and residual pores are perfectly well distributed.

Table 1 Deformation mechanisms in fine grain ceramic polycrystals

n	p	Invoked mechanism	Ref.
1	2	Nabarro-Herring: VD	[31]
1	3	Coble: GBD	[32]
1	2	Superplasticity: GBS + VD [$(d\varepsilon/dt) = 7[(d\varepsilon/dt)_{N-H}]$	[33]
1	3	Superplasticity: GBS + GBD [$(d\varepsilon/dt) = 7(d\varepsilon/dt)_C$]	[33]
1	3	GBS + (IR/GBD): diffusion control [$(d\varepsilon/dt) = (d\varepsilon/dt)_C/22$]	[34]
2	2	GBS + (IR/GBD): IR control	[34]
1	2	GBS + (IR/VD): diffusion control [$(d\varepsilon/dt) = (d\varepsilon/dt)_{N-H}/7$]	[34]
2	1	GBS + (IR/VD): IR control	[34]
1	1	GBS + DDP: dissolution–precipitation reaction control	[35]
1	3	GBS + DDP: diffusion in grain boundary glass control	[35]
4	3	GBS + cavities nucleation/growth	[36]
2	?	GBS + preexisting cavities growth	[37]

GBS: grain boundary sliding; VD: volume diffusion; GBD: grain boundary diffusion; IR: interface reaction; DDP: dissolution–diffusion–precipitation (amorphous grain boundary phase)

Creep tests results

Some general tendencies

Monotone creep tests results at 1,175, 1,200, and 1,225 °C, for different applied true stresses, are shown in Figs. 2, 3, 4, respectively.

Whatever the temperatures and applied stresses, no real steady state is observed, except perhaps for the test performed at 1,200 °C under 40 MPa. In most cases, the creep rate decreases with strain. For tests done at 1,225 °C under 150 and 200 MPa, the creep rate decreases until 40% of deformation and begins to increase again after that. Most of the time this kind of behavior is associated with damage of the sample material during creep deformation (cavities formation, cracks generation, and propagation...).

It also has to be noted that in most cases (1,175 °C/all stresses, 1,200 °C/100 and 150 MPa, 1,225 °C/100 and 150 MPa), the creep rate seems to decrease more or less linearly as an exponential function of the creep strain.

The final densities of the monotonous deformed samples are seen in Fig. 5. For the samples deformed at 1,175 °C, in comparison with the as-sintered material, the relative density is substantially increased when the applied stresses are 100 and 150 MPa. For the same temperature, the relative density of the sample crept under 200 MPa is higher than the relative density of the as-sintered material, but clearly lower than the ones of the samples deformed under 100 and 150 MPa. When the creep temperature is 1,200 °C, the final density of the deformed samples is strongly increased for an applied stress equal to 40 and 100 MPa. When the stress increases to 150 MPa, the final relative density of the crept sample is higher than the as-sintered one, but clearly lower than the ones of the samples deformed under 40 and 100 MPa. Finally, when the applied stress is 200 MPa, the crept sample

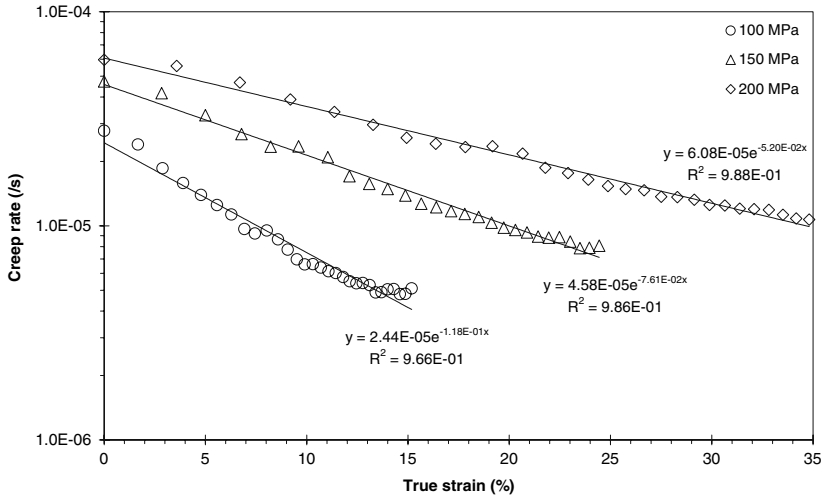

Fig. 2 Creep rate—T = 1,175 °C

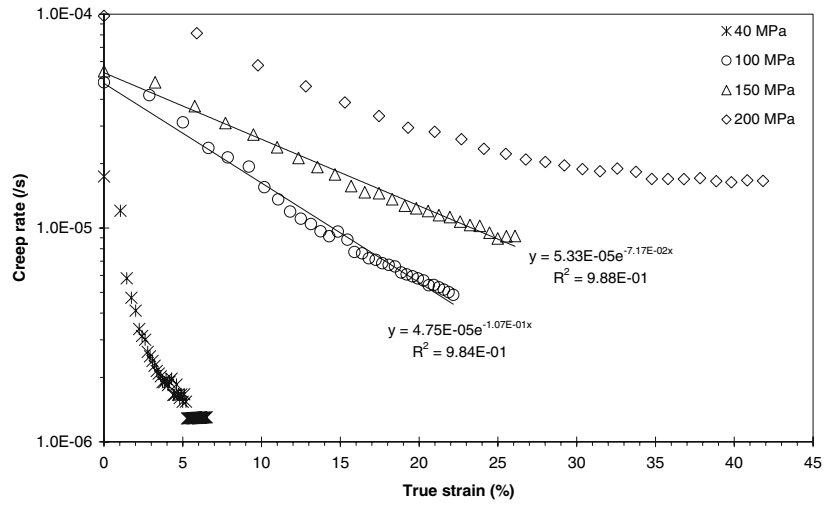

Fig. 3 Creep rate—T = 1,200 °C

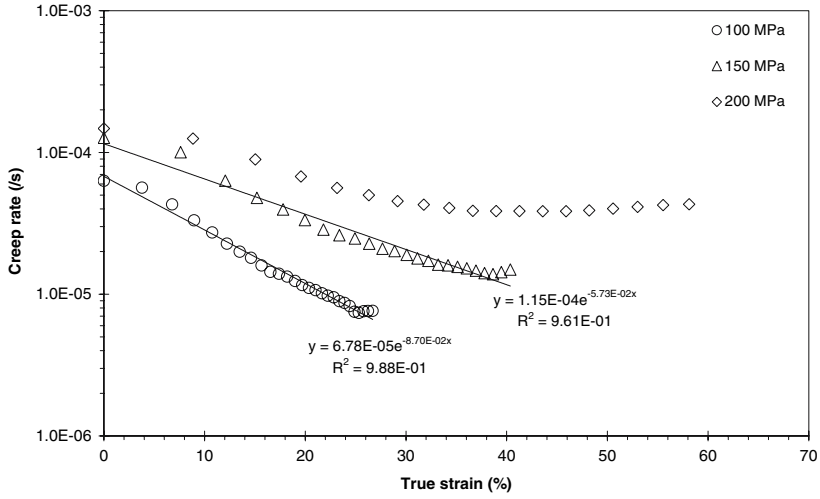

Fig. 4 Creep rate—T = 1,225 °C

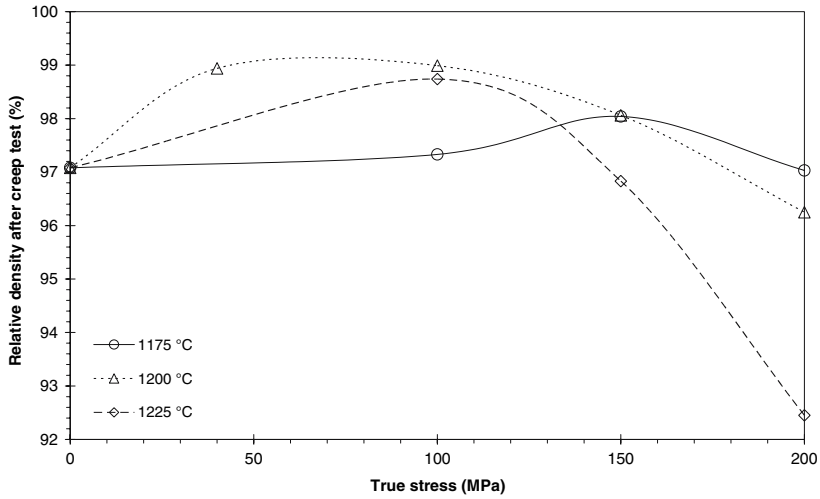

Fig. 5 As-crept relative densities

has a relative final density lower than the one measured on the as-sintered material. So, at 1,200 °C, the relationship between the crept samples relative density versus the applied true stress adopts a bell curve behavior. When the creep temperature is 1,225 °C, this kind of bell curve behavior is much more pronounced. In particular, when creep tests are performed with an applied pressure of 200 MPa, the relative final density of the deformed sample is clearly much lower than the one measured on the as-sintered material. Without going very deeply in details at this point (see Sect. 4 for details) it clearly seems that two mechanisms are involved during the creep deformation of the as-sintered material retained for this study. When the applied stress and/or the temperature is low, creep deformation leads to samples having an increased relative density compared to the as-sintered material. Conversely, when the applied stress and/or the temperature is high, damage occurs and progresses during creep which leads to crept samples having a lower relative density than that of the as-sintered material.

Creep parameters

To identify the mechanism governing the creep deformation at high temperature of the as-sintered material, it is critical to have access to the n, p and Q_d values which are the main parameters involved in relation (1).

Figures 6 and 7 show the evolution of creep rate as a function of creep strain during stress jumps experiments performed at 1,150 and 1,200 °C, respectively. It is now possible to calculate the different instantaneous n values for each stress jump and both creep temperatures. The average n values are 2.0 ± 0.1 and 1.8 ± 0.1 at 1,150 and 1,200 °C, respectively. Therefore, in all cases, whatever the temperature or the stress jump condition, the average n value is very close to 2.

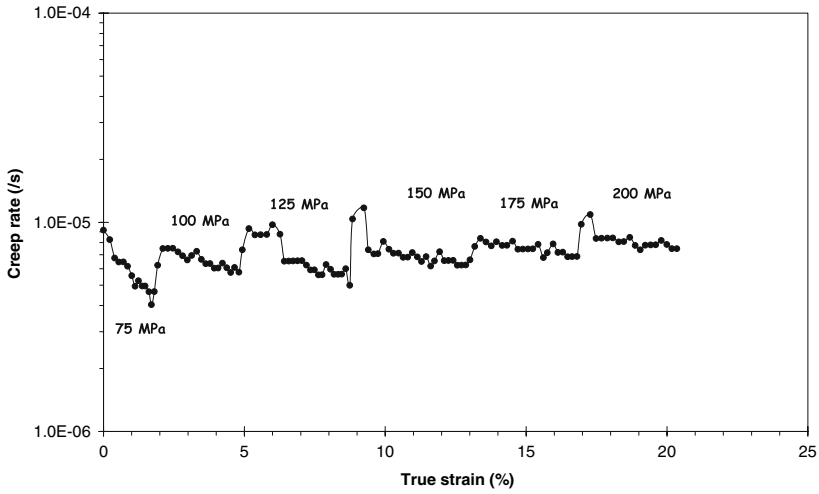

Fig. 6 Stress jumps—T = 1,150 °C

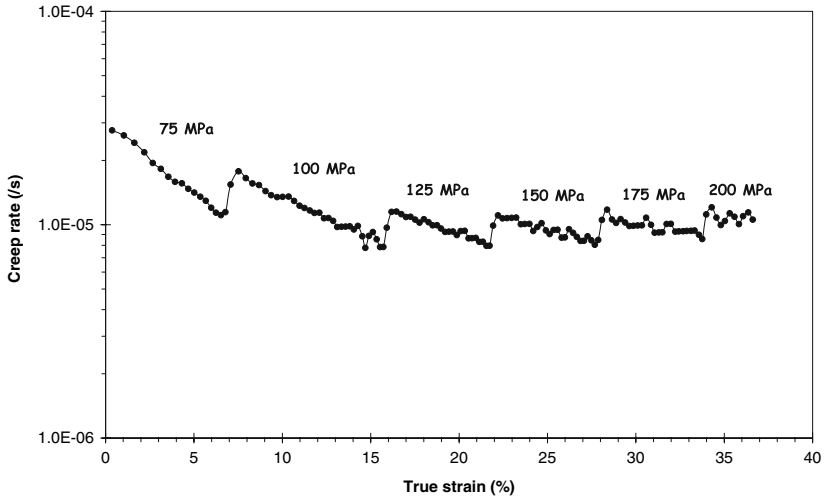

Fig. 7 Stress jumps—T = 1,200 °C

Figure 8 represents the evolution of creep rate as a function of creep strain during temperature jump experiments performed with an applied true stress of 200 MPa. In this case, it is possible to calculate the instantaneous activation energy values for the mechanism controlling the creep deformation at high

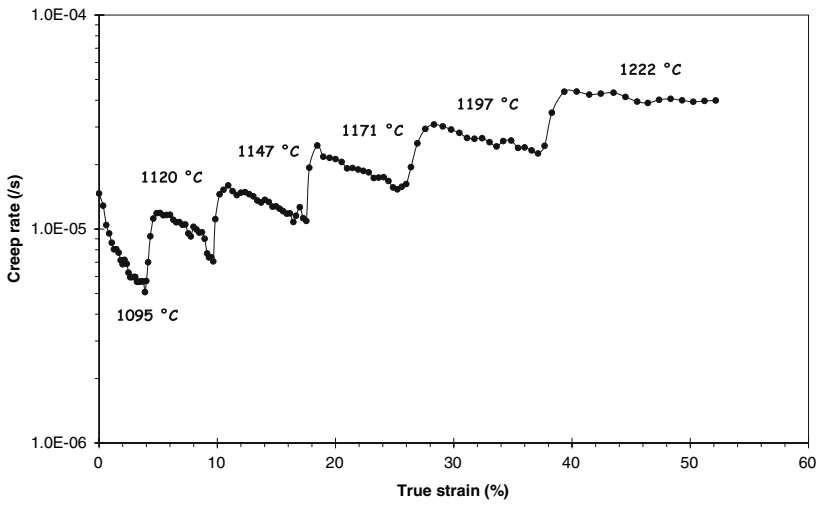

Fig. 8 Temperature jumps—σ = 200 MPa

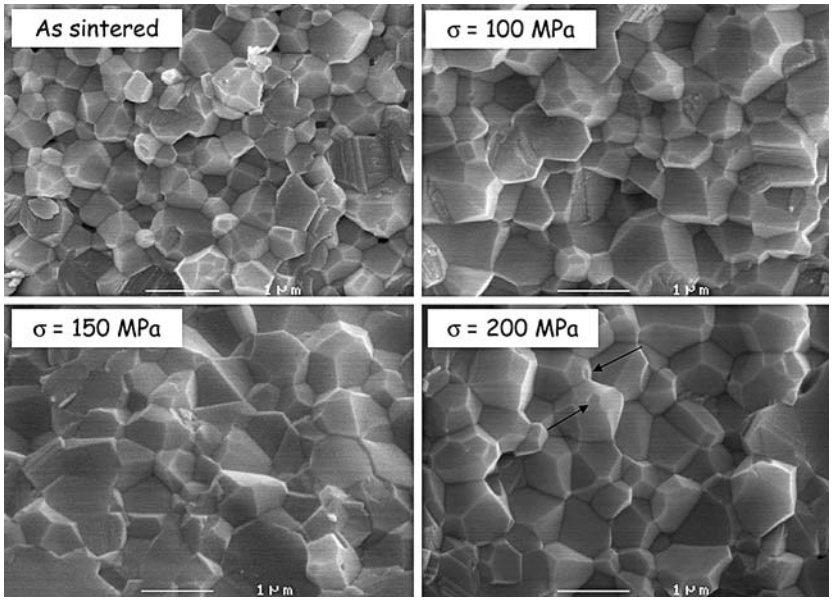

Fig. 9 Microstructure after creep tests—T = 1,175 °C

temperature. Using such a method, an average Q_d value of 488 ± 28 kJ/mol is finally calculated for an applied stress equal to 200 MPa.

Figures 2–4 (by using the different exponential regressions indicated), in conjunction with relation (2), allow the different values for parameter p to be calculated. The average calculated value for p is 5.3 ± 1.4. It is important to note that particularly high and non-conventional values (between 4.1 and 8.4) are reported, probably because no real steady state is reached whatever are the creep conditions.

Microstructure after compressive creep tests

From Figs. 9, 10, 11, we can observe the microstructure evolution after creep as a function of the temperature and applied stress during the tests, compared to the as-sintered one. Key findings are summarized below:

– For all the creep temperatures and the applied stresses, grain growth during high-temperature deformation is evident. Its influence on creep rate has to be taken into account. To evaluate the stress influence on grain size, the average grain size after

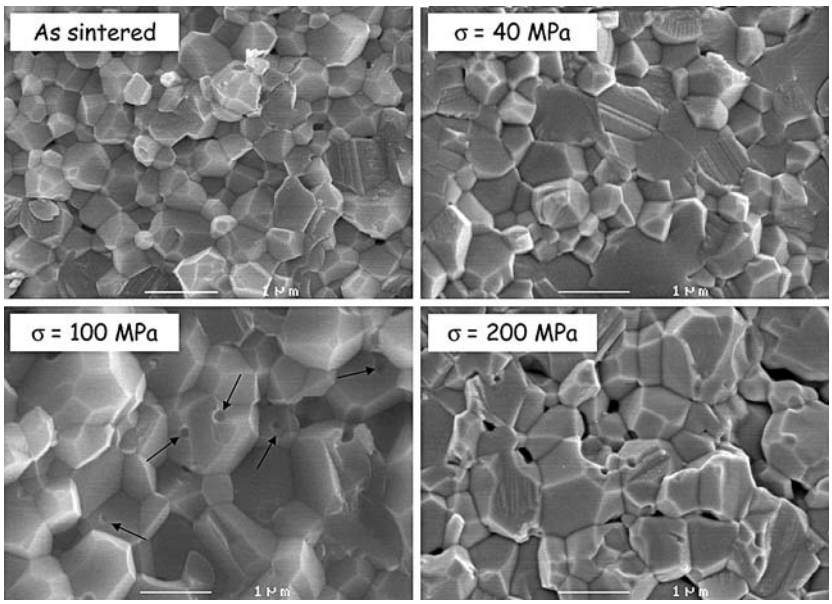

Fig. 10 Microstructure after creep test—T = 1,200 °C

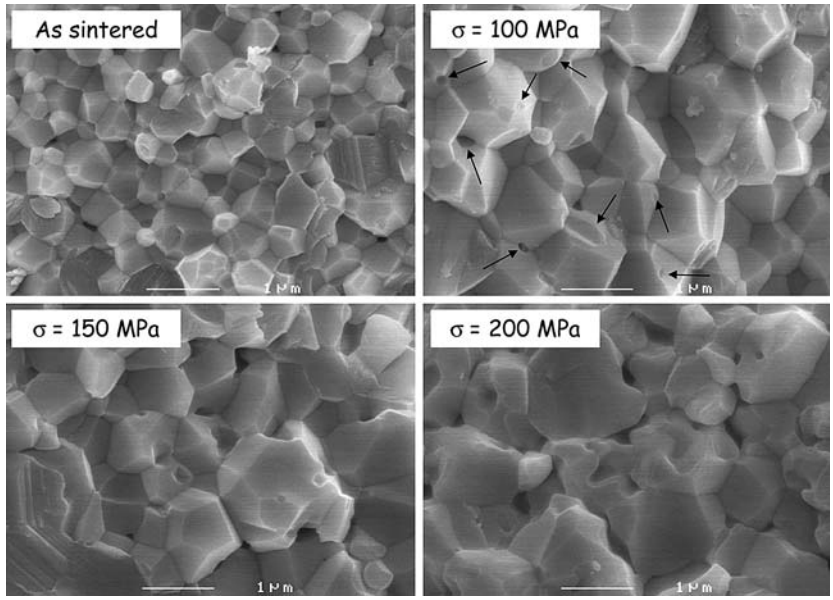

Fig. 11 Microstructure after creep tests—T = 1,225 °C

creep test at 1,200 °C under a stress of 200 MPa was compared to a reference sample put in the creep furnace, without load, at the same time. The grain size in the witness sample was 0.48 μm versus 0.56 μm for the crept sample. In comparison with the as-sintered sample (grain size equal to 0.42 μm), the grain size increase is 14.3% for the reference sample versus 33.3% for the crept sample. This clearly means that dynamic grain growth is effective during all the creep experiments performed in this study;

- At 1,175 °C (see Fig. 9), when the applied stress is equal to 100 and 150 MPa, the final microstructure, when compared to the as-sintered one, exhibits fewer residual pores (in agreement with Fig. 5) and coarser grains. When the creep stress is 200 MPa, if the grains are still coarser, some rare cavities are detected again at grain boundaries (arrows);
- At 1,200 °C (see Fig. 10), when the applied stress is 40 MPa, the resultant microstructure after creep is coarser compared to the as-sintered one and very few residual pores are observed (in agreement with Fig. 5). When the creep stress is higher, between 100 and 200 MPa, the microstructure continues to coarsen but it is important to note that cavities reappear (arrows), similar to what was observed on the sample deformed at 1,175 °C under an applied compressive stress of 200 MPa;
- When the creep temperature is 1,225 °C (see Fig. 11), the higher the applied stress, the coarser the final microstructure. In comparison with the as-sintered microstructure, it is also evident that when the compressive applied stress is between 100 and 200 MPa many cavities appear during creep deformation (arrows). In the worst case (200 MPa), it is evident that most of the cavities have coalesced. These observations are in agreement with the results explained earlier from Figs. 4 (the creep rate increases at the end of the test) and 5 in Sect. 3.2.1;
- At all temperatures and applied creep stresses, the creep related cavities seem to have a different shape and location compared to the pores observed in the as-sintered material. In the as-sintered microstructure, the cavities have a polygonal geometry and are located mainly at the grains triple points. In the crept samples, most of them have a lenticular or penny shape and are usually located at the alumina grain boundaries.

Discussion

It is difficult to identify the mechanism controlling the high-temperature creep deformation of a material if one of the three key parameters n, p and Q_d in relation (1) is missing.

From experimental creep curves, we have previously determined the apparent "p" values. As mentioned previously in Sect. 3.2.2, they are particularly high (5.3 ± 1.4 in average) probably because no steady state is reached whatever are the creep conditions.

Since dynamic and static grain growth are effective during all the creep tests performed (this is proved by the grain size analysis of crept samples deformed at 1,200 °C under 200 MPa, a witness sample put in the same furnace without load and an as-sintered sample,

as previously reported in Sect. 2.2.3). These two sub mechanisms have to be taken into account to understand the general deformation mechanism governing creep of the ultra pure and slightly porous alumina material selected.

Table 2 summarizes the final sample creep strain, grain size and corresponding creep duration for each creep temperature and monotone creep test. Using ''LAB Fit Curve Fitting Software'' [38], the grain size was fitted with the real creep strain and creep time, for each sample. The three relations obtained for the three different temperatures are:

$$G_{1175\,^\circ\mathrm{C}}(\mu\mathrm{m}) = \frac{\varepsilon\,(\%)}{0.4087\times10^{3} - 0.3554\times10^{-2}t^{2}\,(\mathrm{min})} + 0.4220/R^{2} = 0.9977 \quad (3)$$

$$G_{1200\,^\circ\mathrm{C}}(\mu\mathrm{m}) = \frac{\varepsilon\,(\%)}{0.1775\times10^{3} - 0.2517\times10^{-3}t^{2}\,(\mathrm{min})} + 0.4204/R^{2} = 0.9965 \quad (4)$$

$$G_{1225\,^\circ\mathrm{C}}\,(\mu\mathrm{m}) = \frac{\varepsilon\,(\%)}{0.1557\times10^{3} - 0.9133\times10^{-3}t^{2}\,(\mathrm{min})} + 0.4193/R^{2} = 0.9970 \quad (5)$$

In the previous equations, it is important to note that when $t = 0$ and $\varepsilon = 0$ the corresponding grain size in all cases is close to 0.42 μm, which is consistent with the average grain size of the as-sintered material before any creep deformation.

For a constant creep temperature, a constant creep stress, and a unique value of the activation energy for the mechanism controlling creep, relation (1) is rewritten as follows:

$$\ln(\dot{\varepsilon}_{\mathrm{qs}}) = K - p\ln(G) \quad (6)$$

where K is a constant.

By using relations (3)–(5), it is now possible to plot, point by point, the variation of $\ln(\dot{\varepsilon}_{\mathrm{qs}})$ as a function of $\ln(G)$ for each creep test performed. The results obtained for creep temperatures of 1,175, 1,200 and 1,225 °C are shown in Figs. 12, 13, 14, respectively.

According to expression (6), the relation between $\ln(\dot{\varepsilon}_{\mathrm{qs}})$ and $\ln(G)$ should be linear, the slope value being $-p$. In fact, for all creep temperatures and creep stresses, it is apparent that there are three different linear portions (plain, dashed and dashed/point lines).

Table 3 summarizes, for each creep test, creep temperature and stress, the corrected grain size exponent p values corresponding to the three linear portions. The critical grain size, G^{*}, marking the transition between the plain and dashed linear portions is also indicated.

It is important to note that:

– At the beginning of the creep tests, the sensitivity of creep rate to grain size seems to be very high. The corrected grain size exponent values are between 3 and 22. At this time, it is not possible to identify a corresponding standard deformation mechanism which fits with the previous models summarized in Table 1.

Table 2 Values introduced in the LAB Fit solver to calculate ''G'' in function of ''ε'' and ''t''

	1,175 °C	1,200 °C	1,225 °C
0 MPa	G = 0.42 μm ε = 0% t = 0 min	G = 0.42 μm ε = 0% t = 0 min	G = 0.42 μm ε = 0% t = 0 min
40 MPa	–	G = 0.48 μm ε = 6.58% t = 468 min	–
100 MPa	G = 0.58 μm ε = 15.35% t = 296 min	G = 0.56 μm ε = 22.42% t = 328 min	G = 0.71 μm ε = 27.04% t = 268 min
150 MPa	G = 0.59 μm ε = 24.80% t = 268 min	–	G = 0.82 μm ε = 40.69% t = 234 min
200 MPa	G = 0.65 μm ε = 34.81% t = 270 min	G = 0.69 μm ε = 42.65% t = 258 min	G = 0.88 μm ε = 58.62% t = 182 min

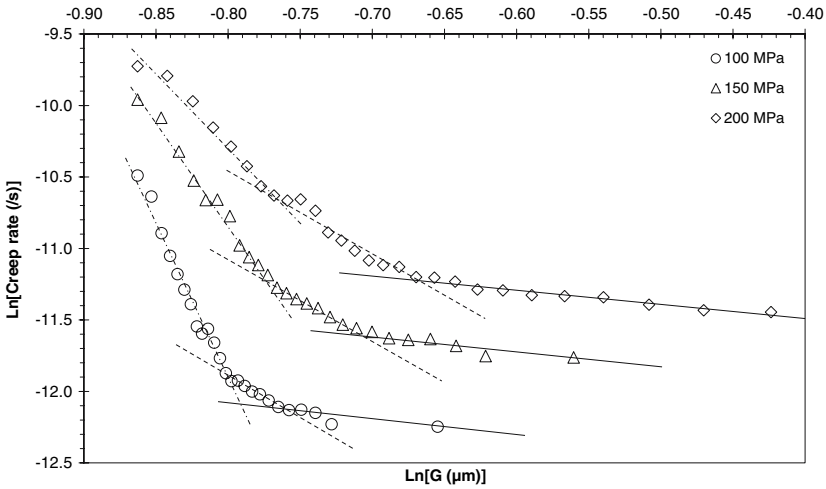

Fig. 12 Relation between creep rate and grain size—T = 1,175 °C

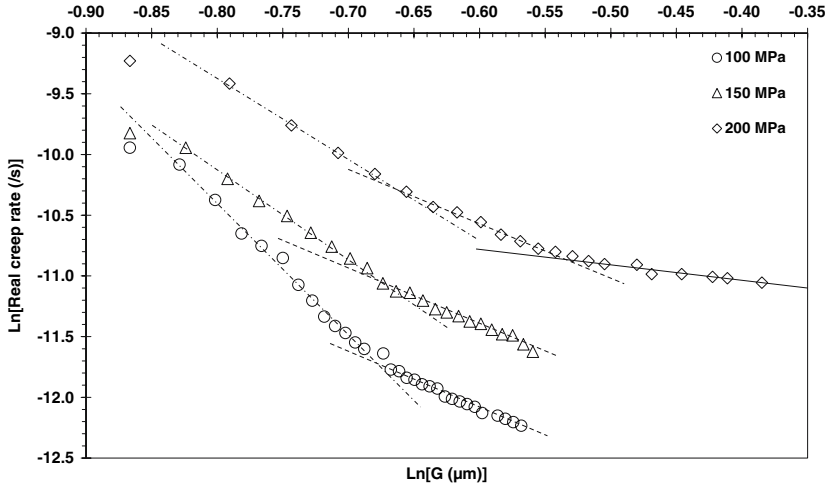

Fig. 13 Relation between creep rate and grain size—T = 1,200 °C

– When the grain size becomes higher than G^*, the different p values are very close to 1, for all creep temperatures and stresses. It should also be noted that the average value of G^*, $\langle G^* \rangle$, is more or less constant at a given creep temperature, for all creep stresses. It is also interesting to observe that $\langle G^* \rangle$ is increasing linearly with the creep temperature, as can be seen in Fig. 15.

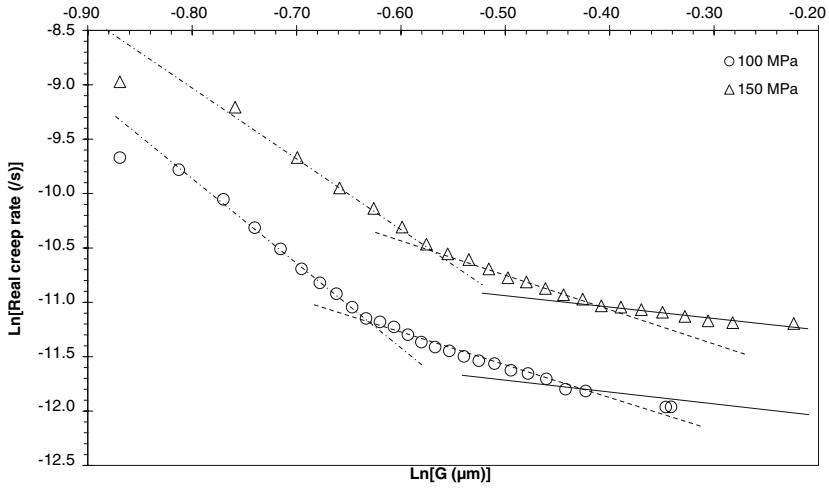

Fig. 14 Relation between creep rate and grain size—T = 1,225 °C

Table 3 Corrected grain size exponent, p

	1,175 °C	1,200 °C	1,225 °C
100 Mpa	Dashed & point line → $p \approx 21.5$ Dashed line → $p \approx 6.0$ Plain line → $p \approx 1.1$ $G^* \approx 0.45$ μm	Dashed & point line → $p \approx 10.6$ Dashed line → $p \approx 4.6$ Plain line → ? $G^* \approx$?	Dashed & point line → $p \approx 7.7$ Dashed line → $p \approx 3.0$ Plain line → $p \approx 1.2$ $G^* \approx 0.66$ μm
150 Mpa	Dashed & point line → $p \approx 14.1$ Dashed line → $p \approx 5.7$ Plain line → $p \approx 1.1$ $G^* \approx 0.49$ μm	Dashed & point line → $p \approx 7.5$ Dashed line → $p \approx 4.5$ Plain line → ? $G^* \approx$?	Dashed & point line → $p \approx 6.4$ Dashed line → $p \approx 3.1$ Plain line → $p \approx 1.1$ $G^* \approx 0.66$ μm
200 Mpa	Dashed & point line → $p \approx 10.4$ Dashed line → $p \approx 5.9$ Plain line → $p \approx 1.0$ $G^* \approx 0.51$ μm	Dashed & point line → $p \approx 6.6$ Dashed line → $p \approx 4.7$ Plain line → $p \approx 1.2$ $G^* \approx 0.59$ μm	–

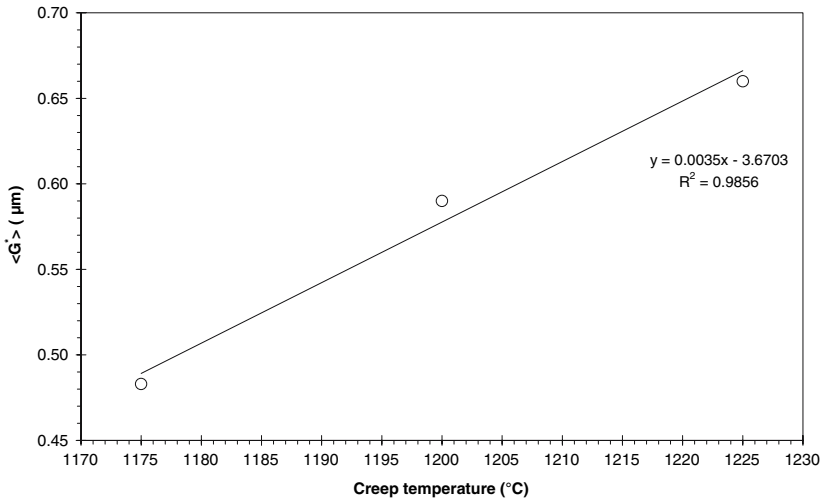

Fig. 15 Relation between $\langle G^* \rangle$ and creep temperature

The Q_d and n values were previously calculated and reported in Sect. 3.2.2. The primary results are:

- For creep temperatures equal to 1,150 and 1,200 °C and an applied compressive stress between 75 and 200 MPa, n is in all cases very close to 2;
- When the applied creep stress is 200 MPa and the temperature between 1,095 and 1,222 °C, the average value for Q_d is 488 ± 28 kJ/mol. It should be noted that this value is very close to the one corresponding to the lattice (or volume) diffusion of Al^{3+} in polycrystalline alumina which is 477 kJ/mol.

Table 1 shows that only three deformation mechanisms can be invoked when the stress exponent value is 2. These mechanisms are:

a. Grain boundary sliding accommodated by an in-series {interface-reaction/grain boundary diffusion} mechanism controlled by the interface-reaction step [34];
b. Grain boundary sliding accommodated by an in-series {interface-reaction/lattice diffusion} mechanism controlled by the interface-reaction step [34];
c. Grain boundary sliding accommodated by the growth of preexisting cavities [37].

The average corrected grain size exponent value has been shown to be very close to 1 in all deformation conditions (temperature and stress) when the grain size becomes higher than a critical value $\langle G^* \rangle$. Thus, when looking at Table 1, the deformation mechanism referred in point (a) can be eliminated. Finally only mechanisms (b) and (c) can be responsible for controlling the high-temperature compressive creep deformation of the as-sintered material in the temperature and stress ranges adopted there.

When considering these key deductions with the microstructure observation results (see Sect. 3.2.3), it seems relatively evident that the two deformation mechanisms exposed in (b) and (c) are effective when the grain size exceeds $\langle G^* \rangle$. We can say that:

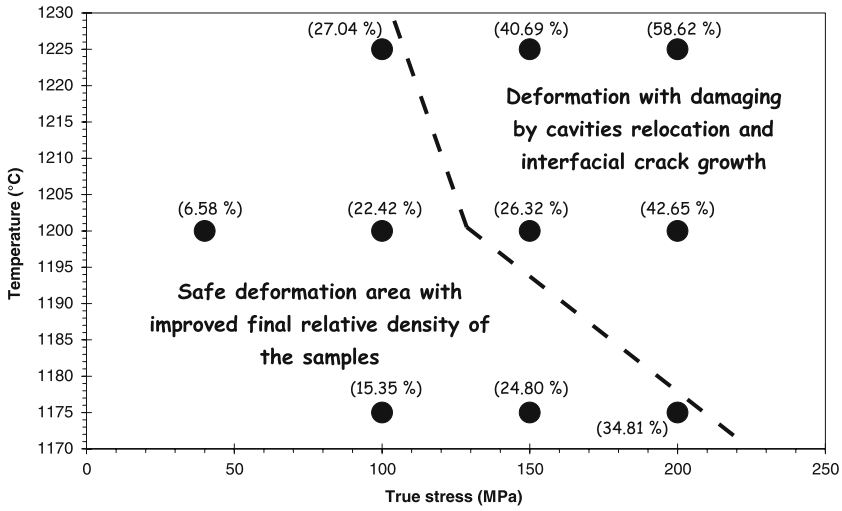

Fig. 16 Creep mechanisms—transition border

– For low stresses and/or low temperatures, which are related to an increase in the crept samples densities in comparison with the as-sintered one and associated values of $n = 2$ and $p = 1$, the compressive creep deformation proceeds by grain boundary sliding accommodated by an in-series {interface-reaction/lattice diffusion of the Al^{3+} cations} mechanism controlled by the interface-reaction step. This is in very good agreement with the expression derived from Burton's calculation [34]:

$$\dot{\varepsilon}_s^{\text{Burton}} \approx \xi(T)\frac{\sigma^2 e^{-\frac{Q_v}{RT}}}{G} \tag{7}$$

where $\xi(T)$ is a constant for a fixed creep temperature and $Q_v = Q_d$ represents the activation energy for the lattice (or volume) diffusion of the migrating species,

– For high stresses and/or high temperatures, which are related to a decrease in the crept samples densities in comparison with the as-sintered one and also associated values of $n = 2$ and $p = 1$, the compressive creep deformation proceeds by grain boundary sliding accommodated by the relocation and interfacial crack growth of preexisting cavities (non-optimal sintering). The growth step is also controlled by the diffusion of Al^{3+} cations. This suggestion seems to be in agreement with the equation derived from Suresh's work [37], although his final equation does not incorporate the standard creep parameters "p" and "Q_d".

Finally, Fig. 16 summarizes the transition border between one deformation mechanism and an other as a function of the temperature and applied stress for the as-sintered slightly porous (D = 97.2%) submicron alumina material selected. In order to obtain "safe" near net shape final pieces by uniaxial superplastic forming pre-sintered compacts, it is necessary to use conditions (temperature and applied stress) shown on the left side of the dashed border. At this point, it is important to note that Fig. 16 is only valid for the total amount of strain indicated for each creep experiment (values in percentage between brackets). If one particular creep experiment is prolonged or shortened in time (which means that the total amount of strain is higher or lower than the one indicated on Fig. 16 and also that the grain size is different from the one indicated in Table 2), it is possible that the dashed border line on Fig. 16, separating the two deformation region, is not valid anymore.

In order to minimize residual pores in the final near net shape pieces after superplastic forming and to have a shaping rate higher than 10^{-5}/s, the following parameters: $T = 1{,}175$ °C and $\sigma = 150$ MPa are recommended.

Conclusion

Compressive creep tests in air were performed on a polycrystalline submicron as-sintered and slightly porous α-alumina material. Two different deformation mechanisms, depending on the applied stress and creep temperature, have been identified when the grain size exceeds a critical value $\langle G^* \rangle$. In contrast, when the grain size is lower than $\langle G^* \rangle$ no known deformation mechanism can be proposed for the control of creep deformation. In this case the sensitivity of the creep rate to grain size is very high.

Using the results obtained, it is possible to identify the optimal conditions for high-temperature uniaxial superplastic forming previously as-sintered parts, leading to shaped objects having an increased final density

compared to the as-sintered ones. In order to minimize the residual porosities in the final objects and to have, at the same time, a shaping rate always higher than 10^{-5}/s (for optimization of the industrial yield in the case of final products having a high profitability), the recommended experimental parameters are: T = 1,175 °C and σ = 150 MPa.

References

1. Krell A, Blank P, Ma H, Hutzler T, Nebelung M (2003) J Am Ceram Soc 86(4):546
2. Krell A, Blank P, Ma H, Hutzler T, van Bruggen MPB, Apetz R (2003) J Am Ceram Soc 86(1):12
3. Munro RG (1997) J Am Ceram Soc 80(8):1919
4. Schacht M, Boukis N, Dinjus E (2000) J Mater Sci 35(24):6251
5. Mikeska KR, Bennison SJ (1999) J Am Ceram Soc 82(12):3561
6. Oda K, Yoshio T (1997) J Am Ceram Soc 80(12):3233
7. Dogan CP, Hawk JA (1999) Wear 225–229(2):1050
8. Kalin M, Novak S, Vizintin J (2003) Wear 254(11):1141
9. Bataille A, Addad A, Crampon J, Duclos R (2005) J Eur Ceram Soc 25(6):857
10. Bataille A, Crampon J, Duclos R (1999) Ceram Int 25(3):215
11. Xue LA, Chen IW (1996) J Am Ceram Soc 79(1):233
12. Wang ZC, Davies TJ, Ridley N, Ogwu AA (1996) Acta Mater 44(11):4301
13. Clarisse L, Baddi R, Bataille A, Duclos R, Vicens J (1997) Acta Mater 45(9):3843
14. Flacher O, Blandin JJ, Plucknett KP (1996) Mater Sci Eng A Struct Mater: Prop Microstruct Process 221(1&2):102
15. Bernard-Granger G, Baddi R, Duclos R, Crampon J (1992) J Eur Ceram Soc 10(1):13
16. Dominguez-Rodriguez A, Gomez-Garcia D, Lorenzo-Martin C, Munoz-Bernabe A (2003) J Eur Ceram Soc 23(15):2969
17. Tong GQ, Chan KC, Gao L, Lin ZR (2002) Mater Sci Eng A Struct Mater: Prop Microstruct Process 336(1&2):263
18. Duclos R, Crampon J, Carry C (2002) Philos Mag Lett 82(10):529
19. Charity I, Chokshi AH (2001) Acta Mater 49(12):2239
20. Jimenez-Melendo M, Dominguez-Rodriguez A (1999) Philos Mag A Phys Condens Mater Struct Defects Mech Prop 79(7):1591
21. Béclin F, Duclos R, Crampon J, Valin F (1997) J Eur Ceram Soc 17(2&3):439
22. Béclin F, Duclos R, Crampon J, Valin F (1995) Acta Metall Mater 43(7):2753
23. Besson JL, Murat D, Rouxel T, Valin F, Boncoeur M (1996) J Am Ceram Soc 79(3):773
24. Rouxel T, Murat D, Besson JL, Boncoeur M (1996) Acta Mater 44(1):263
25. Shinoda Y, Nagano T, Hui Gu F, Wakai F (1999) J Am Ceram Soc 82(10):2916
26. Kondo N, Suzuki Y, Ohji T, Sato E, Wakai F (1999) Mater Sci Eng A Struct Mater: Prop Microstruct Process 268(1&2):141
27. Kondo N, Wakai F (1996) J Mater Sci 31(20):5499
28. Rouxel T, Wakai F, Izaki K (1992) J Am Ceram Soc 75(9):2363
29. Technical data sheet of the TM-DAR raw powder, Taimei Chemicals Co. Ltd, Tokyo, Japan
30. Technical data sheet of the SM8 raw powder, Baïkowski, La Balme de Sillingy, France
31. Herring C (1950) J Appl Phys 21(5):437
32. Coble RL (1963) J Appl Phys 34(6):1679
33. Ashby MF, Verrall RA (1973) Acta Metall 21(2):149
34. Burton B (1983) Phil Mag A 48(3):L9
35. Raj R, Chyung K (1981) Acta Metall 29 (1):159
36. Evans AG, Rana A (1980) Acta Metall 28(2):129
37. Suresh S, Brockenbrough JR (1990) Acta Metall Mater 38(1):55
38. Silva WP, Silva CDPS (1999–2005) LAB Fit Curve Fitting Software (non-linear regression and treatment of data program), V 7.2.33, online, available from world wide web: www.labfit.net